Do binary supracrystals enhance the crystal stability?

Do Binary Supracrystals Enhance the Crystal Stability?

Zhijie Yang,[1] Thomas Altantzis,[2] Sara Bals,[2] Gustaaf Van Tendeloo,[2] Marie-Paule Pileni[3*]

[1] Université Paris Diderot, Sorbonne Paris Cité, ITODYS, UMR 7086 CNRS, 15 rue J-A de Baïf, 75205 Paris, Cedex 13, France

[2] Electron Microscopy for Materials Research (EMAT), University of Antwerp, Groenenborgerlaan 171, 2020 Antwerp, Belgium

[3] Fondation de la Maison de la Chimie, 28 rue Saint Dominique, 75008 Paris, France

* Corresponding author: mppileni@orange.fr

Abstract

We study the oxygen thermal stability of two binary systems. The larger particles are magnetic amorphous Co (7.2 nm) or Fe_3O_4 (7.5 nm) nanocrystals whereas the smaller ones (3.7 nm) are Au nanocrystals. The nanocrystal ordering, as well as the choice of the magnetic nanoparticles very much influence the stability of the binary system. A perfect crystalline structure is obtained with the Fe_3O_4/Au binary supracrystals. For the Co/Au binary system, oxidation of Co results in the chemical transformation from Co to CoO, where the size of the amorphous Co nanoparticles increases from 7.2 to 9.8 nm in diameter. During the volume expansion of the Co nanoparticles, Au nanoparticles within the binary assemblies coalesce and are at the origin of the instability of the binary nanoparticle supracrystals. On the other hand, for the Fe_3O_4/Au binary system, the oxidation of Fe_3O_4 to γ–Fe_2O_3 does not lead to a size change of the nanoparticles, which maintains the stability of the binary nanoparticle supracrystals. A similar behavior is observed for an AlB_2 type Co-Ag binary system: The crystalline structure is maintained, whereas in disordered assemblies, coalescence of Ag nanocrystals is observed.

Introduction

Self-assembly of inorganic nanoparticles into supracrystals or superlattices is of particular interest because of their potential application in new solid-state-material-based devices that have unique electronic, catalytic, optical or magnetic properties.[1-8] In nanoparticle chemistry, an ensemble of colloidal nanoparticles is able to self-assemble into an ordered entity by either evaporation of carrier solvent or diffusion of a bad solvent.[9-12] In the last two decades, binary nanoparticle supracrystals composed of two distinct nanoparticles have been discovered, and tens of crystal structures found in binary metallic alloys have been developed.[13-20] In addition to the crystal phase control of the binary nanoparticle supracrystals, post-synthesis treatment is another strategy to achieve structure-dependent properties, by which either the interparticle distance between nanoparticles within the supracrystals or the chemical composition is modulated.[21-23] For example, Klajn et al. recently developed a strategy based on the selective removal of one type of nanoparticles from binary nanoparticle superlattices, through which non-close-packed nanoparticle arrays can be precisely modulated.[21] Our group and others recently showed that controlled fusion of the adjacent nanoparticle clusters within an AB_{13} or AB_6 binary nanoparticle supracrystal can modulate the crystal structure of the binary nanoparticle supracrystal by post-synthesis thermal treatment.[22,23]

The interdiffusion processes between oxygen and Co nanocrystals, called the nanokirkendall effect, are markedly dependent on the nanocrystallinity and on the size of the nanoparticles. With amorphous Co nanoparticles mainly the pure CoO structure is observed whereas with single domain cubic Co (ε-phase) hollow CoO nanoparticles are produced.[24] With compact structures, such as hcp or fcc, either core/shell or hollow nanoparticles are produced depending on the nanocrystal size and the nanocrystallinity.[25] The oxidation of Fe_3O_4 nanocrystals results in the formation of γ–Fe_2O_3 (maghemite) nanocrystals; however the phase transformation does lead to a significant size change of the ferrite nanocrystals. Here, we demonstrate the importance of the type of large magnetic nanoparticles in order to maintain the crystalline structure of the magnetic (Co or Fe_3O_4)/Au binary supracrystals.

Experimental sections

Chemicals: All materials were used without further purification: cobalt acetate, iron (III) chloride hexahydrate, dodecanethiol, oleic acid, sodium borohydride, toluene,

tert-butylamine borane and methanol are from Aldrich, isooctane from Fluka, ethanol from VWR chemicals, sodium di(ethylhexyl) sulfosuccinate (NaAOT) from Sigma, Chlorotriphenylphosphine Au (I) from Strem chemicals, sodium oleate from T.C.I. . The synthesis of ($Co(AOT)_2$ were described previously.[26]

Apparatus: Conventional transmission electron microscopy was performed using a JEOL 1011 microscope operated at 100 kV. High angle annular dark-field scanning TEM (HAADF-STEM) and STEM energy dispersive X-rays spectroscopy (STEM-EDS) measurements were performed using an aberration-corrected cubed FEI-Titan electron microscope operated at 200 kV. For the acquisition of the elemental maps, the ChemiSTEM,[27] system was used.

Synthesis of Co nanoparticles: Co nanoparticles were synthesized from reverse micelles, as already described.[28] Briefly, by using mixed reverse micelles of $Co(AOT)_2$ (0.05 M) (40 %) and Na(AOT) (0.1 M) (60 %) in presence of water molecules such $w = [H_2O]/[AOT] = 32$ are reduced by sodium borohydride as ($R = [NaBH_4]/[Co(AOT)_2] = 6$). Co nanoparticles are immediately produced and oleic acid (316 μL) is added to coat the nanoparticles. The coated Co nanoparticles are then washed and centrifuged four times with ethanol to remove the AOT surfactant and the black powder obtained was dispersed in toluene. At the end of the synthesis, 7.2 nm Co nanoparticles coated with oleic acid with a ~ 9 % size distribution were produced. The entire synthesis is carried out in an N_2 glove box using de-oxygenated solvents to prevent particle oxidation. As already observed amorphous-like nanoparticles are obtained.[29]

Synthesis of Fe_3O_4 nanoaprticles: iron oxide nanoparticles were synthesized by slightly modifying the method reported by Hyeon et al.[30] First, iron oleate precursors were prepared as follows: 10.8 g of iron(III) chloride hexahydrate, 36.5 g of sodium oleate, 40 mL of DI water, 40 mL of ethanol, and 80 mL of hexane were mixed into a 500 mL flask. The mixture is refluxed at ~64 ^oC for 4 h. The dark hexane solution was washed 3 times by warm DI water (~50 ^oC) and separated in a separatory funnel. The viscous product is obtained by evaporating the hexane in a rotary evaporator. A stock precursor solution with a concentration of 0.5 mol/kg was prepared by adding 1.5 g of octadecene to each gram of iron oleate. For the synthesis of 7.5 nm Fe_3O_4 nanoparticles, 4.8 g of precursor solution was mixed with 1.0 g oleic acid and with 6.0 g octylether. The mixture was heated to 110 ^oC and maintained at this temperature for 60 min under N_2 protection. Then the solution was heated to the boiling point of the solution (~295 ^oC) and was kept at this temperature for 30 min followed by removal of the heater. The colloidal solution was washed 5 times using

isopropyl alcohol/hexane (1:1 v/v) by sedimenting and redispersing using centrifugation (5000 rpm for 10 min). Finally, the Fe_3O_4 nanoparticles were weighted and redispersed in toluene with desired nanoparticle concentration.

Synthesis of Au nanoparticles: Au nanoparticles with a dimeter of 3.7 nm are synthesized by revisiting the Stucky method.[31] Typically, two solutions are used. One consists of 0.20 mmol of Chlorotriphenylphosphine Au (I) dissolved in 25 mL of toluene to which 500 μL of dodecanethiol (DDT) is added. The other one contains 5 mmol of *tert*-butylamine borane dissolved in 2 mL of toluene. The two solutions are placed in a silicone oil bath at 100 ^oC and are stirred for 10 min. Subsequently *tert*-butylamine borane solution is injected into the solution with gold salt swiftly. The colorless and clear mixture turns to brown and reaches a dark purple red solution in 1 min, and this solution is kept at 100 ^oC for another 4 min followed by the remove of the oil bath. The Au nanoparticles are precipitated from the colloidal solution by adding 10 mL of methanol. The supernatant is removed. The black precipitate is dried in a nitrogen flow in order to eliminate the remaining solvent. The Au nanoparticles are weighted and redispersed in toluene with desired nanoparticle concentration.

Synthesis of Ag nanoparticles: Ag nanoparticles coated with dodecanethiol ($C_{12}H_{25}SH$) are synthesized by the reverse micelles method: the water content, w = $[H_2O]/[AOT]$, is kept at 2. Hydrazine dispersed in 0.1 M Na(AOT) is added to the mixed micelles. Dodecanethiol used as coating agent, is then added to the reverse micelles containing the nanoparticles. To remove the AOT surfactant, ethanol is added to the solution. After washing four times with ethanol, nanoparticles with a mean diameter of 4.0 nm and a size distribution of 9 % were obtained, which were re-dispersed in toluene.

Supracrystals Growth: Self-assembly of binary colloidal solution is carried out in an experimental setup shown in elsewhere published before,[32] and the temperature can be controlled (*i.e.* 45^oC in the present study). Ultra-thin carbon-coated copper TEM grids were used as the substrate for self-assembly experiments. The grids were placed inside a glass vial with inner diameter of ~4 mm. Then 40 μL of solution containing a mixture of Co (or Fe_3O_4) and Au nanoparticles with the desired particle ratio, keeping the overall particle concentration constant 5.8×10^{-7} M, was injected into the glass vial. The solution was evaporated under N_2 atmosphere, avoiding any oxidation of Co nanoparticles.

Oxidation of binary nanoparticle supracrystals: TEM grids loaded with binary nanoparticle supracrystals were placed into the oxidation apparatus, which is assembled based on the Schlenk line, including high-vacuum pump, source of inert gas (Ar) and

source of oxygen gas (O_2).[29] The sample was first submitted to Ar flux and evacuate to remove the air. Then O_2 flow was conducted before placing a heating setup that was preset to 200 ^oC. The samples were kept at 200 ^oC for 15 min before removing the heating source and replacing the Ar flow in order to stop the oxidation instantly.

Results and discussion

Amorphous Co nanoparticles coated with oleic acid (C_{18}) with an average diameter of 7.2 ± 0.6 nm are produced from reverse micelles; this was already described previously[28]. A mixture of single and polycrystalline Au nanocrystals (3.7 ± 0.3 nm) coated with dodecanothiol is produced using the Stucky method.[31] The effective nanoparticle size, d_{eff}, is defined as the center to center distance between nanoparticles that are self-ordered in a compact hexagonal network, i.e. the sum of the metal core diameter and twice the thickness of the organic ligand. These data are obtained from the representative TEM images. Considering the surface ligand coating, the effective diameters of Co and Au nanoparticles are 10.2 nm and 5.7 nm, respectively. According to the hard sphere model, the system adopts the crystal structure corresponding to the most efficient space filling, to reach the maximum packing density ρ for a given ratio of the sphere radii γ.[33] The parameter γ = 0.56 is defined as the effective diameter ratio of the Au versus the Co nanoparticle ($\gamma = d_{Aueff}/d_{Coeff}$). According to the phase diagram, this γ value favors the formation of either AlB_2-type or $NaZn_{13}$-type binary crystals[33]. From our previous data[32] we know that the final structure also depends on the relative concentration ratio between [Au]/[Co]. With [Au]/[Co] = 2, a long range ordered AlB_2-type (space group *P6/mmm*) $CoAu_2$ binary crystal is to be expected (**Figure 1b).** This is confirmed by the TEM image in **Figure 1a** as well as by the HAADF-STEM image in **Figure 1c**. Both images show that the nanoparticles are highly ordered and form $CoAu_2$ supracrystals. The bright and dark regions in the HAADF-STEM image correspond to elemental Au (Z = 79) and Co (Z = 27) respectively. From the STEM-EDS elemental maps (**Figures 1d-1f)** it is clear that the Au nanocrystals are ordered into a "honeycomb" structure, whereas the Co nanoparticles are assembled into the cavities of the Au honeycombs. Note that in some region of the TEM grid, disordered assemblies are also observed.

The $CoAu_2$ supracrystals, deposited on a carbon coated copper TEM grid, are placed in a modified Schlenk-line setup, submitted to an oxygen flux and baked at 200 ^oC.

After 15 min at 200 ^{o}C, the heating source is removed and argon gas is introduced so as to stop the drastic oxidation at once.

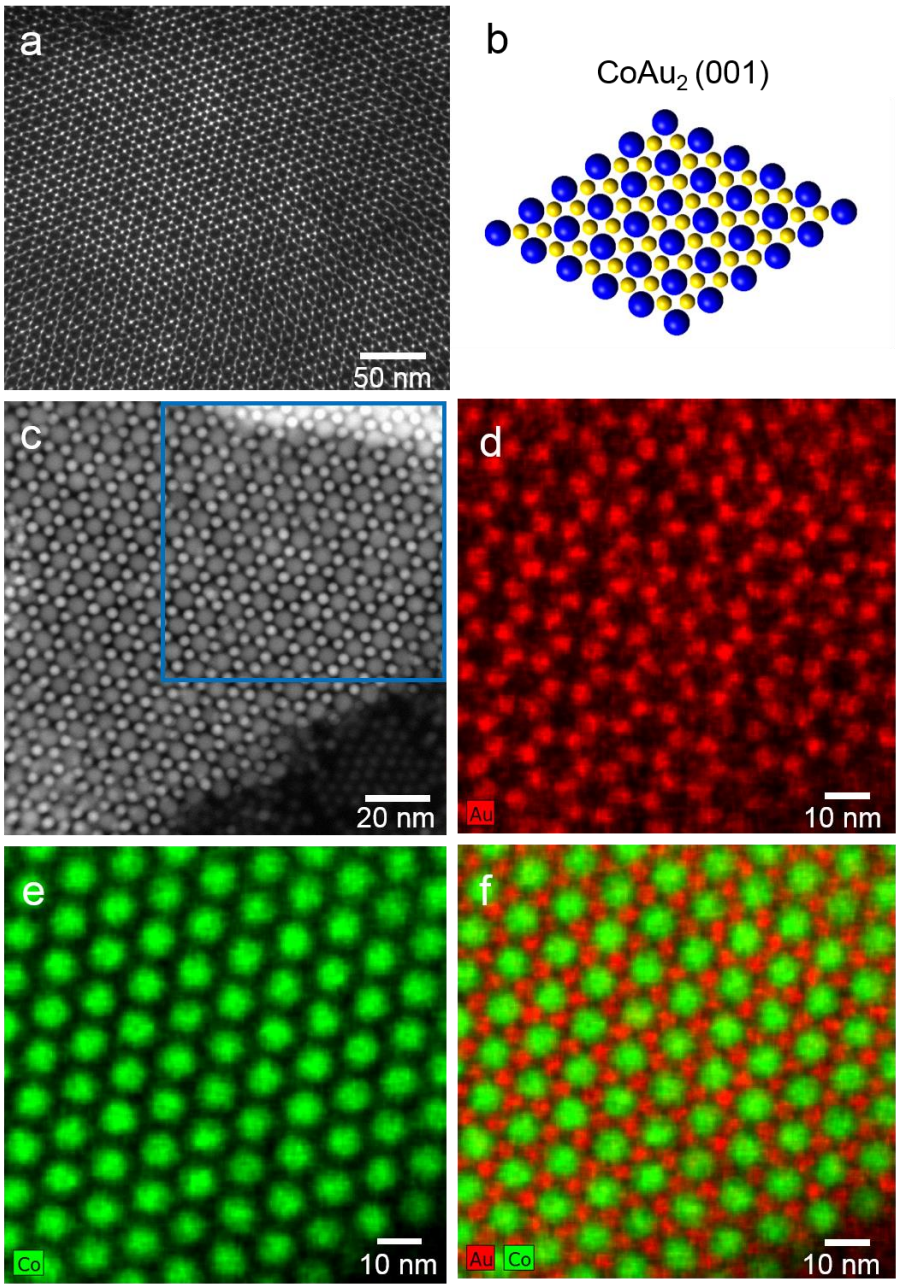

Figure 1. **a**, TEM image of binary nanoparticle supracrystals with AlB_2-type $CoAu_2$; **b**, crystal model of $CoAu_2$ with (001) crystal plane; **c**, HAADF-STEM image of the $CoAu_2$ binary nanoparticle supracrystals; **d-f**, STEM-EDS elemental maps acquired from the region indicated by the blue square in **c**, in which the distribution of the elements in the structure can be observed (Au and Co in red and green respectively).

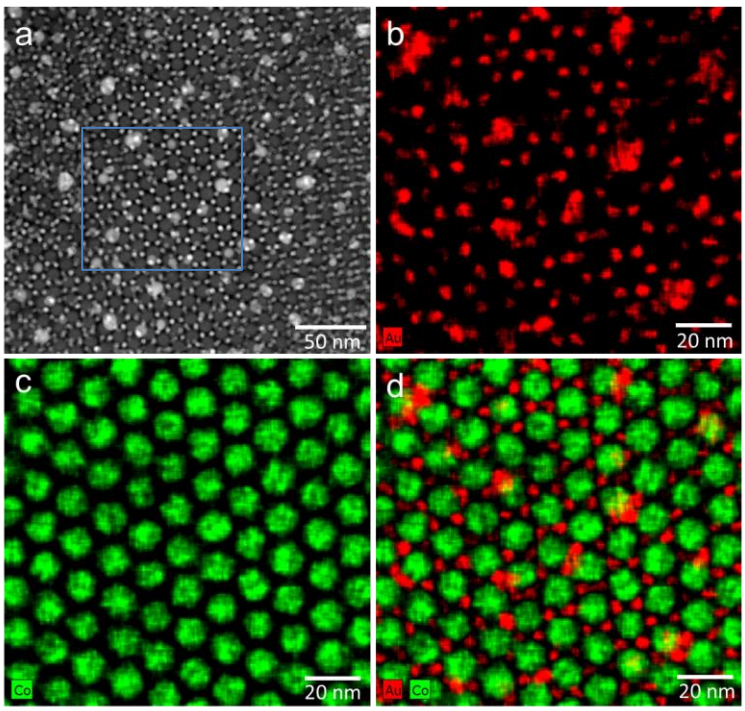

Figure 2. a, HAADF-STEM image of an ordered area in the Co-Au sample after the oxidation; **b-d**, STEM-EDS elemental maps acquired from the region indicated by the blue square in **a**, in which the distribution of the elements in the structure can be observed (Au and Co in red and green respectively)**.**

Figure 2a shows that the material with the high Z value i.e Au tends to aggregate whereas the Co maintains its integrity. The STEM-EDS elemental maps indeed confirm that part of the Au nanocrystals (**Figure 2b**) sinter into larger particles whereas another part remains stable after oxidation. In previous studies[29] we demonstrated that amorphous Co nanoparticles, self assembled in 2D superlattices, produce either cubic CoO or core/shell Co/CoO nanocrystals inducing an increase in the nanoparticle size leading to the formation of a less dense structure (cubic).[29] The cobalt elemental mapping in **Figure 2c** shows that the thermally treated $CoAu_2$ superlattice forms a hexagonal close packed structure of the Co. **Figure** 2d confirms the presence of small and large Au nanoparticles whereas the CoO nanoparticles keep their uniform size. The average diameter of Co to CoO nanoparticles evolves from 7.2 nm to 9.8 nm. This is related to the oxidation of the Co nanoparticles to CoO. These data are consistent with those obtained by thermal treatment of Co nanocrystals under the same experimental conditions, self assemblied in 2D superlattices (**Figures** 3a and 3b). Co nanoparticles remains self assembled in a compact hexagonal network with most nanoparticles having a homogeneous contrast. Note that few of them show a dark core, characteristic of a core/shell structure. In comparison, Au nanocrystals

are markedly unstable and fuse under thermal treatment **(Figures** 3c and 3d). The fusion of Au nanoparticles can be due to the heating-induced shringkage of superlattices.[34-36]

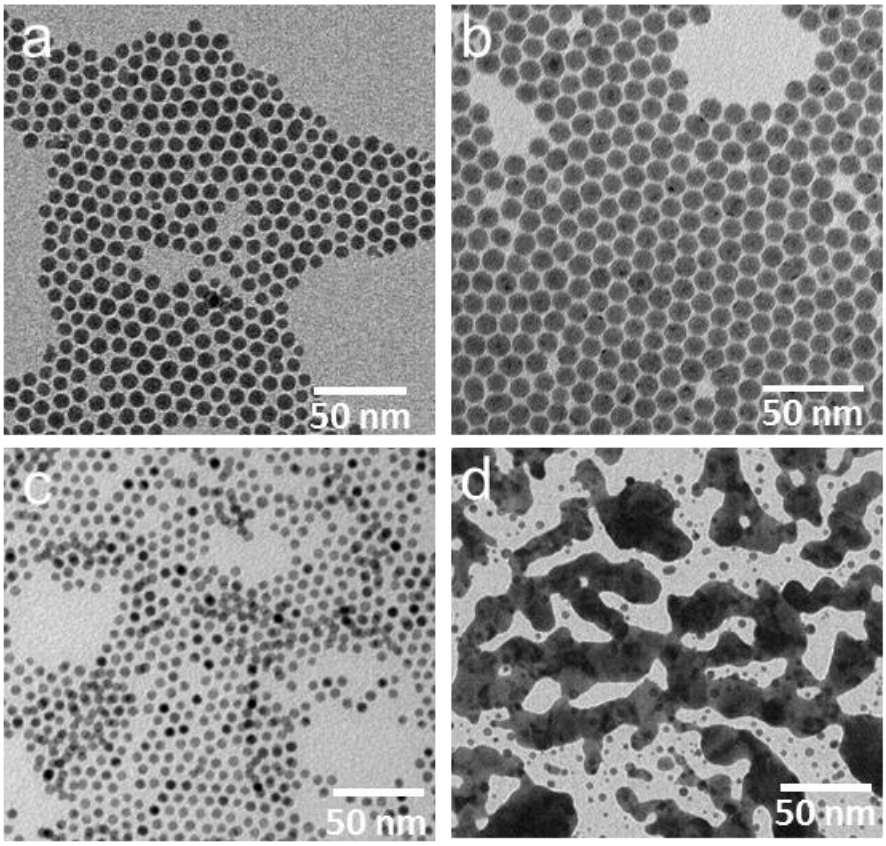

Figure 3. TEM images of Co nanoparticles before (**a)** and after (**b**) thermal treatment; **(c),(d)** TEM images of Au nanoparticles before (**c**) and after (**d**) thermal treatment in oxygen flow at 200 ^{o}C for 15 min.

In some regions the Co/Au binary system is disordered (**Figures 4a and 4b**). **Figures 4c-4f** show, as previously, an increase in the Co nanoparticle size due to the formation of CoO and confirm the sintering of Au nanocrystals into larger nanoparticles (from 7nm up to 30nm). This clearly shows some immunity to thermal treatments. In fact, it is well known that the thermal stability of isolated nanoparticles is remarkably reduced because of the melting-point-depression phenomena.[37] On increasing the temperature, the interparticle mass transport of isolated nanoparticles induces the formation of a "bridge" between the nanoparticles. These "bridges" tend to relax into a spherical shape, driven by the minimization of the surface energy. In the Co/Au disordered regions, the Co nanoparticles remain immune to the thermal treatment whereas the Au nanocrystals tend to sinter into larger particles (from 7 up to 30 nm); similar to the ordered binary supracrystals.

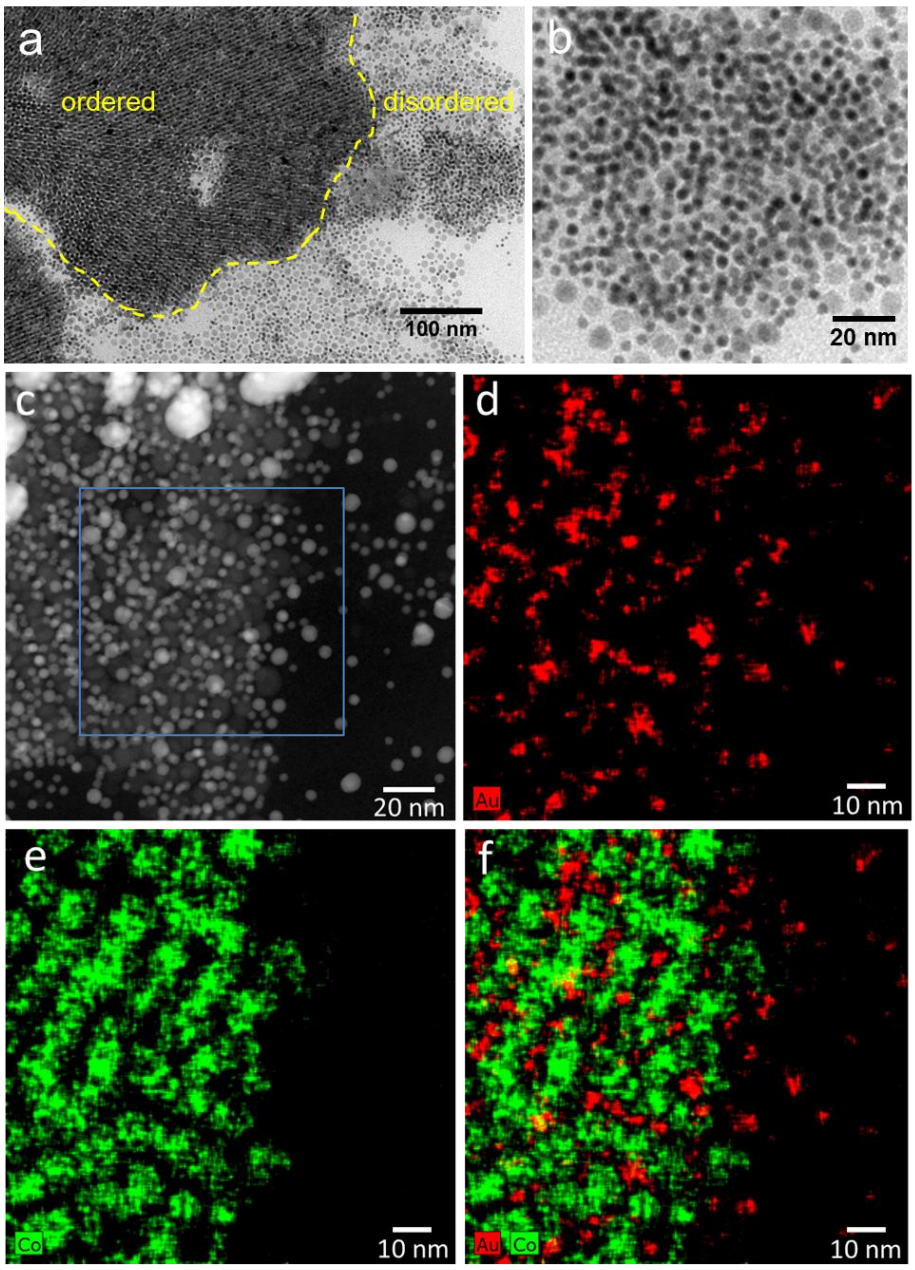

Figure 4. a,**b**, TEM image of a disordered area in a Co-Au binary sample; **c**, HAADF-STEM image of an amorphous area in a Co-Au sample after oxidation; **d-f**, STEM-EDS elemental maps acquired from the region indicated by the blue square in **c**, in which the distribution of the elements in the structure can be observed (Au and Co in red and green respectively) .

Replacing Co (7.2 ± 0.6 nm) by Fe_3O_4 (7.5 ± 0.6 nm) nanoparticles, while keeping all other parameters (concentration ratio, growth temperature, etc…) constant, a similar AlB_2 type crystalline structure is produced. The TEM image of the $(Fe_3O_4)Au_2$ binary supracrystal **(Figure** 5a) is in very good agreement with the crystal model along (001) crystal plane (**Figure** 5b). The HAADF-STEM image (Figure 5c) as well as the STEM-EDS mapping confirms (**Figures** 5d-5e) the Fe_30_4 and Au nanocrystals ordering. This

clearly shows that under fixed experimental conditions (concentration, temperature, γ value etc…) long-range order of binary supracrystals is produced. The $(Fe_3O_4)Au_2$ binary nanoparticle supracrystals are submitted to the same thermal treatment as described above for $CoAu_2$ (deposition on a carbon coated copper TEM grid, placed in a modified Schlenk-line setup, submited to oxygen flux and baked at 200 ^oC during 15min). **Figure** 6 shows a perfect similarity of the patterns observed before (**Figure** 5) and after (Figure 6) thermal treatment. Note that here Au nanocrystals keep their integrities and remain ordered.

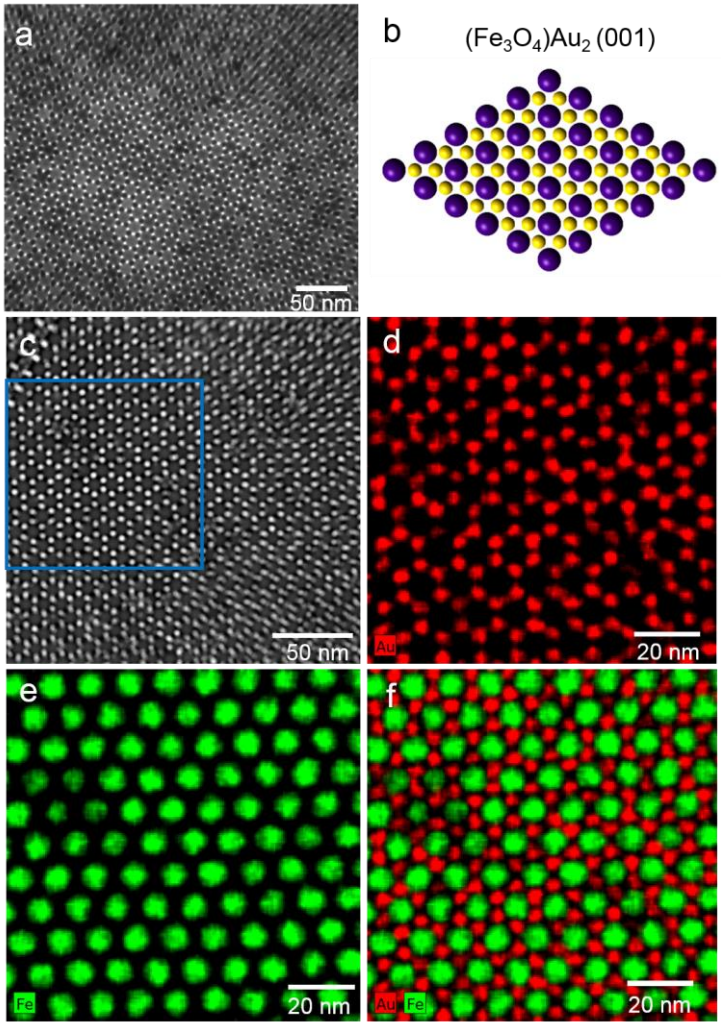

Figure 5. a, TEM image of binary nanoparticle supracrystals with the AlB_2-type $(Fe_3O_4)Au_2$; **b**, (001° plane model of the $(Fe_3O_4)Au_2$ structure; **c**, HAADF-STEM image of a $(Fe_3O_4)Au_2$ binary nanoparticle supracrystal; **d-f,** STEM-EDS elemental maps acquired from the region indicated by the blue square in **c**, in which the distribution of the elements in the structure can be observed (Au and Fe in red and green respectively).

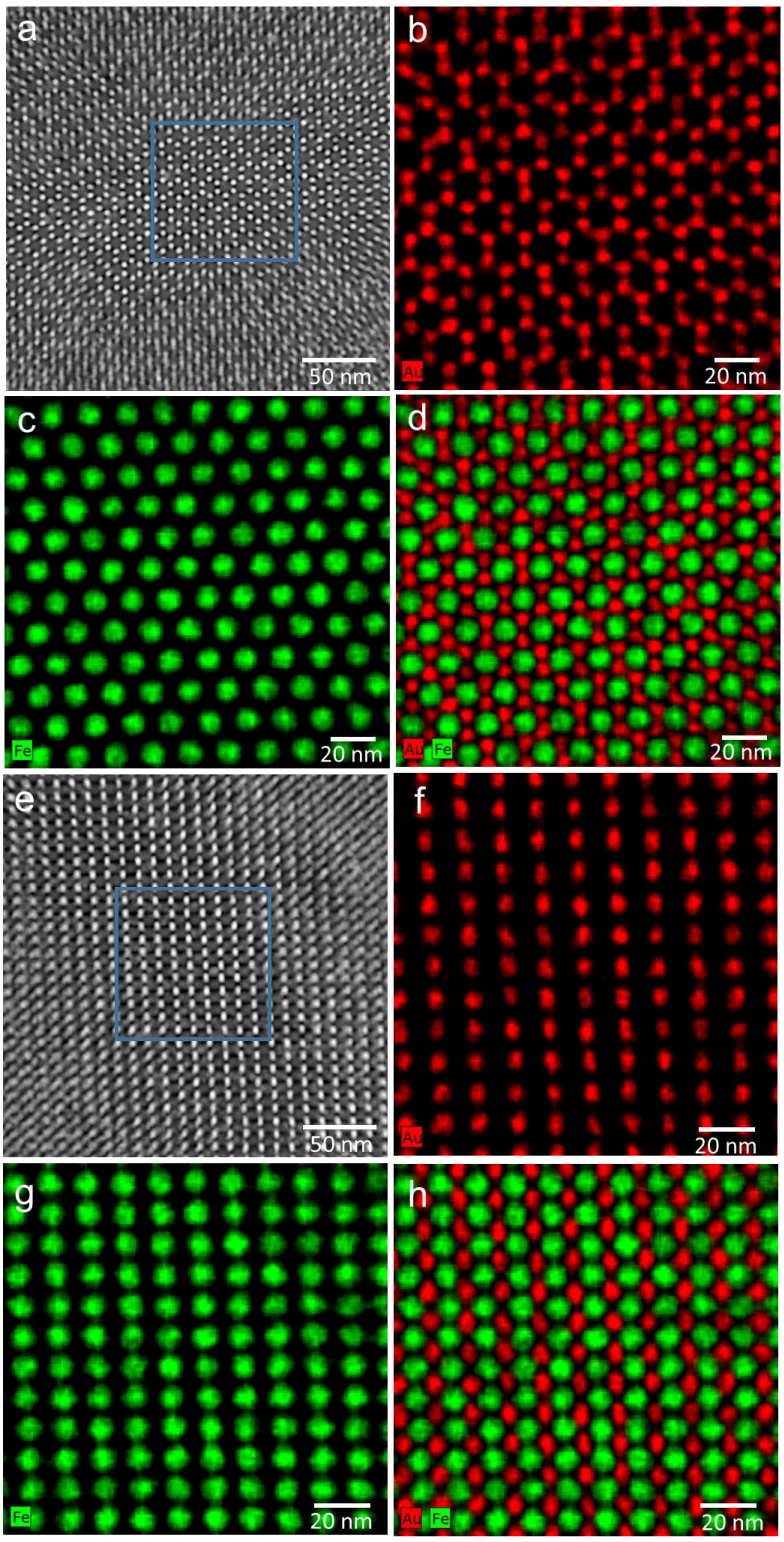

Figure 6 a, HAADF-STEM [001] view of $(FeO_x)Au_2$ after the oxidation; **b-d**, STEM-EDS elemental maps acquired from the region indicated by the blue square in **a**, in which the distribution of the elements in the structure can be observed (Au and Fe in red and green respectively)**. e,** HAADF-STEM [110] view of $(FeO_x)Au_2$ after the oxidation; **f-h**, STEM-EDS elemental maps acquired from the region indicated by the blue square in **e**, in which the distribution of the elements in the structure can be observed (Au and Fe in red and green respectively)**.**

Independent of the orientation of the structure of the $(FeO_x)Au_2$ binary assembly after oxidation, the nanocrystals maintain their initial position in the structure. Therefore it is concluded that the binary structure involving ferrite/Au is maintained. Note that, opposite to the Co/Au binary system, Au nanocrystals are no longer sintering. They keep their configuration. At this point we have to note that even though the crystalline structure of Fe_3O_4 is maintained some change in composition is to be expected: Fe_3O_4 (magnetite) and γ–Fe_2O_3 (maghemite) nanocrystals have a similar crystal structure with similar lattice parameters (8.33Å and 8.36Å respectively) making them very difficult to differentiate.[38] The major difference between γ–Fe_2O_3 and Fe_3O_4 is related to the presence or not of Fe^{2+} in the crystals. It is reasonable to assume that by thermal treatment Fe_3O_4 transforms into γ–Fe_2O_3, keeping similar latttice parameters. Therefore it is logical to conclude that by thermal treatment $(Fe_3O_4)Au_2$ binary supracrystals are replaced by a $(\gamma$–$Fe_2O_3)Au_2$ structure. We also wondered what would be the behavior of the binary strctures when the nanoparticles are not well ordered. Therefore we observed the behavior of the final structure after thermal treatment of a disordered $(Fe_3O_4)Au_2$ binary system.

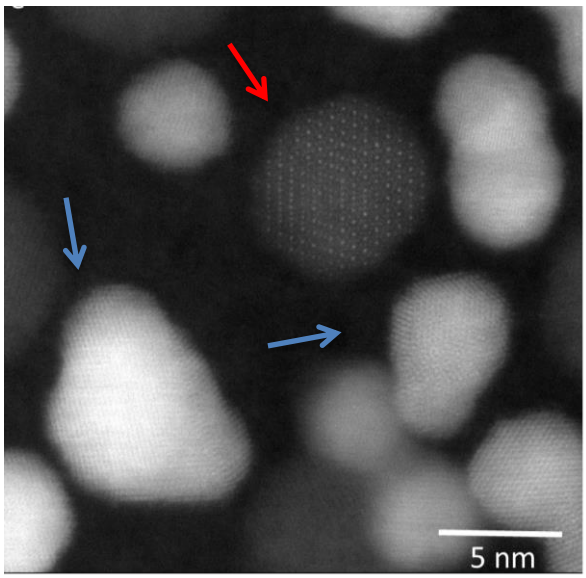

Figure 7. HAADF-STEM image of an amorphous area in the Fe_3O_4-Au sample, where the fused Au (brighter contrast features) and Fe_3O_4 (dark contrast features) nanoparticles are indicated by blue and red arrows respectively.

Figure 7 clearly shows that in disordered $(Fe_3O_4)Au_2$ binary supracrystals, Au nanocrystals fuse leading to the formation of large particles whereas Fe_3O_4 nanocrystals maintain their

crystalline structure, with a potential/probable internal transformation from Fe_3O_4 to γ–Fe_2O_3. We therefore conclude that in order to keep the integrity of the Au nanocrystals the $(Fe_3O_4)Au_2$ binary supracrystals have to be highly ordered; defects induce fusion of the Au nanocrystals. Similar behavior is observed for Co-Ag binary systems. By keeping the same experimental conditions which were described for the Co-Au binary system, a AlB_2 type structure is produced (**inset Figure 8a**). By subjecting such assembly to oxygen flux at 200°C, the crystalline structure remains unchanged (**Figure 8a**), whereas in the corresponding amorphous area Ag nanoparticles coalesce to form larger nanocrystals and CoO nanoparticles are produced (**Figure 8b**). We have to note that if Au instead of Ag nanocrystals are used, the AlB_2 binary structure is not maintained. (**Figure 1**). This can be attributed to the different behaviour of Au and Ag nanocrystals upon exposure to oxygen, where they fuse (**Figure 3d**) or coalesce to larger particles (**Figure S1**) respectively. Here, the $CoAg_2$ binary structure is robust against such colaescence process.

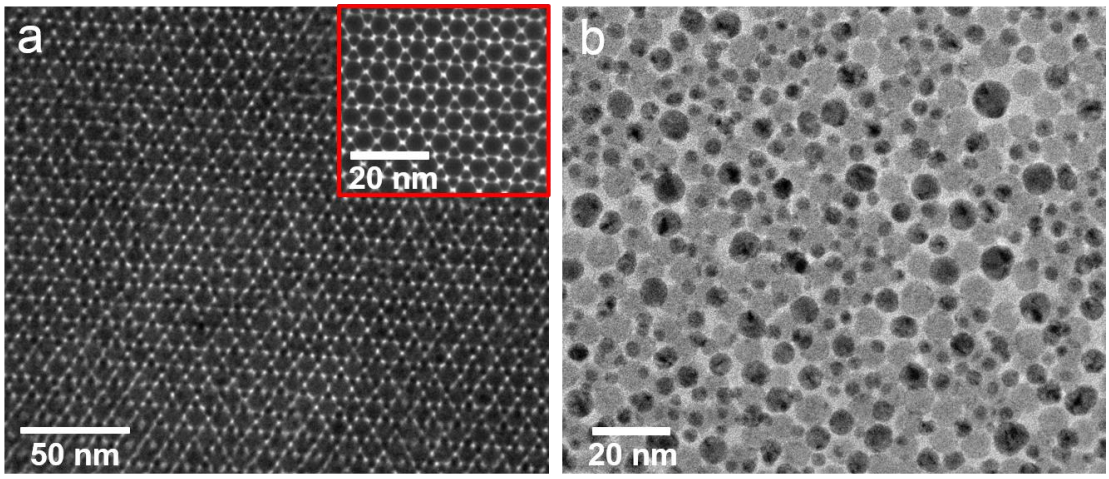

Figure 8. a. AlB_2-type $CoAg_2$ binary superlattices before (inset) and after the oxidation treatment at 200°C for 15 min. **b**. Random aggregate of Co-Ag binary mixtures after the oxidation treatment at 200°C for 15 min.

Conclusions

We have produced two types of binary nanoparticle supracrystals that have the same AlB_2 crystal structure. The thermal stability of the binary nanoparticle supracrystals has been investigated. We demonstrated that both Co and Fe_3O_4 keep their morphology intergrities. As already demonstrated[29], an oxygen thermal treatment of amorphous Co nanoparticles will induce CoO nanoparticles with an increase in size; this increase is due to

the fact that CoO has a cubic structure which is no longer a close packing. The crystalline spinel structure of Fe_3O_4 remains unchanged during the oxidation process. The Fe^{2+} in tetrahedral sites is oxidized to Fe^{3+} and consequently the size of the nanocrystals remains unaltered but a change of composition from Fe_3O_4 to Fe_2O_3 takes place. For the Co-Au binary system, it is reasonably suggested that an enhanced compressive stress appears in the thermal process and thus drives the migration and fusion of Au nanoparticles.[39] For the Au nanocrystals the oxygen thermal treatment of the 2D superlattices involves a fusion of the nanocrystals. In disordered binary systems, Au nanocrystals still tend to fuse into larger Au nanocrystals, whereas the ordered binary systems vary depending on the larger sized nanoparticles. When the larger nanoparticles are chosen to be Co nanoparticles, the oxidation of Co results in the size increase and deterrioate the binary system. In other hand, when Fe_3O_4 nanoparticles are used, the overall stability of binary system maintains. Overall, the nanoparticle size expansion within the binary supracrystals can result in an instability of the crystals, where Au nanoparticles tend to partially coalesce. Hence the choice of magnetic nanoparticles for binary structures and that of small nanoparticles such as Au and Ag nanocrystals could be crucial for potential applications of binary supracrystals in devices.

Acknowledgements

The research leading to these results has been supported by an Advanced Grant of the European Research Council under Grant 267129. The authors appreciate financial support by the European Union under the Framework 7 program under a contract for an Integrated Infrastructure Initiative (Reference No. 262348 ESMI). S.B. acknowledges funding from ERC Starting Grant COLOURATOMS (335078). T.A. acknowledges a post-doctoral grant from the Research Foundation Flanders (FWO, Belgium).

References

1. Boles, M. A.; Engel, M.; Talapin, D. V., Self-assembly of colloidal nanocrystals: from intricate structures to functional materials. *Chem. Rev.* **2016,** *116*, 11220-11289.

2. Cheon, J.; Park, J. I.; Choi, J. S.; Jun, Y. W.; Kim, S.; Kim, M. G.; Kim, Y. M.; Kim, Y. J., Magnetic superlattices and their nanoscale phase transition effects. *Proc. Natl. Acad. Sci. U. S. A.* **2006,** *103*, 3023-3027.

3. Miszta, K.; de Graaf, J.; Bertoni, G.; Dorfs, D.; Brescia, R.; Marras, S.; Ceseracciu, L.; Cingolani, R.; van Roij, R.; Dijkstra, M. et al. Hierarchical self-assembly of suspended branched colloidal nanocrystals into superlattice structures. *Nat. Mater.* **2011,** *10*, 872-876.

4. Geyer, T.; Born, P.; Kraus, T., Switching between crystallization and amorphous agglomeration of alkyl thiol-coated gold nanoparticles. *Phys. Rev. Lett.* **2012,** *109*, 128302.

5. Wang, T.; Wang, X.; LaMontagne, D.; Wang, Z.; Wang, Z.; Cao, Y. C., Shape-controlled synthesis of colloidal superparticles from nanocubes. *J. Am. Chem. Soc.* **2012,** *134*, 18225-18228.

6. O'Brien, M. N.; Jones, M. R.; Mirkin, C. A., The nature and implications of uniformity in the hierarchical organization of nanomaterials. *Proc. Natl. Acad. Sci. U. S. A.* **2016,** *113*, 11717-11725.

7. Kim, Y.; Zhu, J.; Yeom, B.; Di Prima, M.; Su, X. L.; Kim, J. G.; Yoo, S. J.; Uher, C.; Kotov, N. A., Stretchable nanoparticle conductors with self-organized conductive pathways. *Nature* **2013,** *500*, 59-U77.

8. Pileni, M.-P., Impact of the metallic crystalline structure on the properties of nanocrystals and their mesoscopic assemblies. *Acc. Chem. Res.* **2017,** *50*, 1946-1955.

9. Wan, Y. F.; Goubet, N.; Albouy, P. A.; Pileni, M. P., Hierarchy in Au nanocrystal ordering in supracrystals: a potential approach to detect new physical properties. *Langmuir* **2013,** *29*, 7456-7463.

10. Talapin, D. V.; Shevchenko, E. V.; Kornowski, A.; Gaponik, N.; Haase, M.; Rogach, A. L.; Weller, H., A new approach to crystallization of CdSe nanoparticles into ordered three-dimensional superlattices. *Adv. Mater.* **2001,** *13*, 1868-1871.

11. Dong, A.; Chen, J.; Vora, P. M.; Kikkawa, J. M.; Murray, C. B., Binary nanocrystal superlattice membranes self-assembled at the liquid-air interface. *Nature* **2010,** *466*, 474-477.

12. Goubet, N.; Portales, H.; Yan, C.; Arfaoui, I.; Albouy, P. A.; Mermet, A.; Pileni, M. P., Simultaneous growths of gold colloidal crystals. *J. Am. Chem. Soc.* **2012,** *134*, 3714-3719.

13. Shevchenko, E. V.; Talapin, D. V.; Kotov, N. A.; O'Brien, S.; Murray, C. B., Structural diversity in binary nanoparticle superlattices. *Nature* **2006,** *439*, 55-59.

14. Talapin, D. V.; Shevchenko, E. V.; Bodnarchuk, M. I.; Ye, X.; Chen, J.; Murray, C. B., Quasicrystalline order in self-assembled binary nanoparticle superlattices. *Nature* **2009,** *461*, 964-967.

15. Shevchenko, E. V.; Talapin, D. V.; O'Brien, S.; Murray, C. B., Polymorphism in AB(13) nanoparticle superlattices: An example of semiconductor-metal metamaterials. *J. Am. Chem. Soc.* **2005,** *127*, 8741-8747.

16. Ye, X.; Chen, J.; Murray, C. B., Polymorphism in self-assembled ab(6) binary nanocrystal superlattices. *J. Am. Chem. Soc.* **2011,** *133*, 2613-2620.

17. Boneschanscher, M. P.; Evers, W. H.; Qi, W.; Meeldijk, J. D.; Dijkstra, M.; Vanmaekelbergh, D., Electron tomography resolves a novel crystal structure in a binary nanocrystal superlattice. *Nano Lett.* **2013,** *13*, 1312-1316.

18. Kostiainen, M. A.; Hiekkataipale, P.; Laiho, A.; Lemieux, V.; Seitsonen, J.; Ruokolainen, J.; Ceci, P., Electrostatic assembly of binary nanoparticle superlattices using protein cages. *Nat. Nanotechnol.* **2013,** *8*, 52-56.

19. Kalsin, A. M.; Fialkowski, M.; Paszewski, M.; Smoukov, S. K.; Bishop, K. J. M.; Grzybowski, B. A., Electrostatic self-assembly of binary nanoparticle crystals with a diamond-like lattice. *Science* **2006,** *312*, 420-424.

20. Wei, J.; Schaeffer, N.; Pileni, M.-P., Ligand exchange governs the crystal structures in binary nanocrystal superlattices. *J. Am. Chem. Soc.* **2015,** *137*, 14773-14784.

21. Udayabhaskararao, T.; Altantzis, T.; Houben, L.; Coronado-Puchau, M.; Langer, J.; Popovitz-Biro, R.; Liz-Marzán, L. M.; Vuković, L.; Král, P.; Bals, S.et al. Tunable porous nanoallotropes prepared by post-assembly etching of binary nanoparticle superlattices. *Science* **2017,** *358*, 514-518.

22. Altantzis, T.; Yang, Z. J.; Bals, S.; Van Tendeloo, G.; Pileni, M. P., Thermal stability of CoAu13 binary nanoparticle superlattices under the electron beam. *Chem. Mater.* **2016,** *28*, 716-719.

23. Treml, B. E.; Lukose, B.; Clancy, P.; Smilgies, D.-M.; Hanrath, T., Connecting the particles in the box - controlled fusion of hexamer nanocrystal clusters within an AB6 binary nanocrystal superlattice. *Sci. Rep.* **2014,** *4*, 6731.

24. Yang, Z.; Yang, N.; Pileni, M.-P., Nano kirkendall effect related to nanocrystallinity of metal nanocrystals: influence of the outward and inward atomic diffusion on the final nanoparticle structure. *J. Phys. Chem. C* **2015,** *119*, 22249-22260.

25. Yang, Z.; Yang, N.; Yang, J.; Bergstroem, J.; Pileni, M.-P., Control of the oxygen and cobalt atoms diffusion through co nanoparticles differing by their crystalline structure and size. *Adv. Funct. Mater.* **2015,** *25*, 891-897.

26. Petit, C.; Taleb, A.; Pileni, M. P., Cobalt nanosized particles organized in a 2D superlattice: Synthesis, characterization, and magnetic properties. *J. Phys. Chem. B* **1999,** *103*, 1805-1810.

27. Schlossmacher, P.; Klenov, D. O.; Freitag, B.; von Harrach, H. S., enhanced detection sensitivity with a new windowless XEDS system for AEM based on silicon drift detector technology. *Microscopy Today* **2010,** *18*, 14-20.

28. Yang, Z.; Cavalier, M.; Walls, M.; Bonville, P.; Lisiecki, I.; Pileni, M.-P., A phase-solution annealing strategy to control the cobalt nanocrystal anisotropy: structural and magnetic investigations. *J. Phys. Chem. C* **2012,** *116*, 15723-15730.

29. Yang, Z.; Lisiecki, I.; Walls, M.; Pileni, M.-P., Nanocrystallinity and the ordering of nanoparticles in two-dimensional superlattices: controlled formation of either core/shell (Co/CoO) or hollow CoO nanocrystals. *ACS Nano* **2013,** *7*, 1342-1350.

30. Park, J.; An, K. J.; Hwang, Y. S.; Park, J. G.; Noh, H. J.; Kim, J. Y.; Park, J. H.; Hwang, N. M.; Hyeon, T., Ultra-large-scale syntheses of monodisperse nanocrystals. *Nat. Mater.* **2004,** *3*, 891-895.

31. Zheng, N.; Fan, J.; Stucky, G. D., One-step one-phase synthesis of monodisperse noble-metallic nanoparticles and their colloidal crystals. *J. Am. Chem. Soc.* **2006,** *128*, 6550-6551.

32. Yang, Z.; Wei, J.; Pileni, M.-P., Metal-metal binary nanoparticle superlattices: a case study of mixing Co and Ag nanoparticles. *Chem. Mater.* **2015,** *27*, 2152-2157.

33. Boles, M. A.; Talapin, D. V., Many-body effects in nanocrystal superlattices: departure from sphere packing explains stability of binary phases. *J. Am. Chem. Soc.* **2015,** *137*, 4494-4502.

34. Li, R.; Zhang, J.; Tan, R.; Gerdes, F.; Luo, Z.; Xu, H.; Hollingsworth, J. A.; Klinke, C.; Chen, O.; Wang, Z., Competing interactions between various entropic forces toward assembly of Pt_3Ni octahedra into a body-centered cubic superlattice. *Nano Lett.* **2016,** *16*, 2792-2799.

35. Wang, Z.; Bian, K.; Nagaoka, Y.; Fan, H.; Cao, Y. C., Regulating multiple variables to understand the nucleation and growth and transformation of PbS nanocrystal superlattices. *J. Am. Chem. Soc.* **2017,** *139*, 14476-14482.

36. Zhang, J.; Zhu, J.; Li, R.; Fang, J.; Wang, Z., Entropy-driven Pt_3Co nanocube assembles and thermally mediated electrical conductivity with anisotropic variation of the rhombohedral superlattice. *Nano Lett.* **2017,** *17,* 362-367.

37. José-Yacamán, M.; Gutierrez-Wing, C.; Miki, M.; Yang, D. Q.; Piyakis, K. N.; Sacher, E., Surface diffusion and coalescence of mobile metal nanoparticles. *J. Phys. Chem. B* **2005,** *109,* 9703-9711.

38. Cornell, R. M.; Schwertmann U. *The iron oxides: structure, properties, reactions, occurrences and uses.* Wiley, Germany, 2003.

39. Zhu, H.; Nagaoka, Y.; Hills-Kimball, K.; Tan, R.; Yu, L.; Fang, Y.; Wang, K.; Li, R.; Wang, Z.; Chen, O., Pressure-enabled synthesis of hetero-dimers and hetero-rods through intraparticle coalescence and interparticle fusion of quantum-dot-Au satellite nanocrystals. *J. Am. Chem. Soc.* **2017,** *139,* 8408-8411.

TOC Graphic

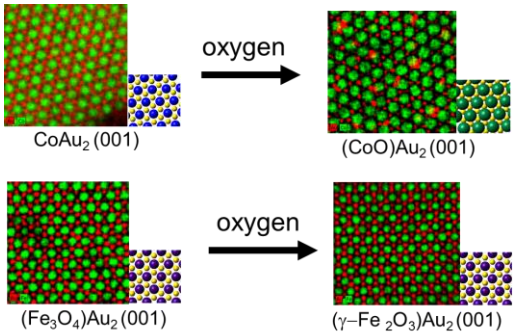
oxygen
$CoAu_2(001)$
$(CoO)Au_2(001)$
oxygen
$(Fe_3O_4)Au_2(001)$
$(\gamma\text{–}Fe_2O_3)Au_2(001)$